Eur J Vasc Endovasc Surg **26**, 649–656 (2003)
doi: 10.1016/j.ejvs.2003.08.004, available online at http://www.sciencedirect.com on SCIENCE DIRECT®

On the Existence of an Optimum End-to-side Junctional Geometry in Peripheral Bypass Surgery—A Computer Generated Study

M. T. Walsh,[1] E. G. Kavanagh,[2] T. O'Brien,[1] P. A. Grace[2] and T. McGloughlin[1]*

[1]*Biomedical Engineering Research Centre, Department of Mechanical and Aeronautical Engineering, University of Limerick, Ireland and* [2]*Mid-Western Regional Hospital, Dooradoyle, Limerick, Ireland*

Background. *To investigate hemodynamic flow changes associated with vein cuffs and patches that may be responsible for improved patency of prosthetic infrainguinal grafts.*
Methods. *The role of the graft–artery junction angle was examined by computational fluid dynamics to assess the influence of anastomotic geometry on wall shear stress (WSS) distributions. Three geometrically different junction configurations were studied and the WSS and WSS gradient (WSSG) values were compared.*
Results. *The inclusion of a patch or a cuff moves the bed stagnation point (BSP) distally, increasing the area on the bed of the junction which experiences a BSP and reducing the strength of the recirculation region opposite the heel of the junction by 54.8 and 50.8%, respectively. The patched geometry promotes earlier recovery of the flow in the distal outflow segment (DOS) than for the unpatched model. Also, the helical flow patterns in the DOS associated with the cuffed geometry are stronger. The net effect of these changes are that peak WSSG values for the patched and cuffed geometries are three times lower than those for the uncuffed geometry.*
Conclusion. *This study provides some additional insights into the hemodynamics of graft–artery junction geometry which may influence future clinical practice.*

Key Words: Anastomosis; Wall shear stress; Computational fluid dynamics; Graft–artery junction.

Introduction

Intimal hyperplasia causing stenosis at the distal anastomosis is a major cause of failure of infrainguinal vascular bypass grafts.[1] It is characterised by the proliferation of vascular smooth muscle cells, under growth factor control, which migrate to cause hyperplasia in the subendothelial plane.[2] Anastomotic restenoses occur predominantly at the heel and toe of the anastomosis and on the artery bed, opposite the anastomosis.[3–5] Disease formation at the suture line can be attributed to three major factors, namely surgical injury, material mismatch and the abnormal flow patterns around the anastomosis. However, disease formation on the bed of the junction is thought to be entirely due to the abnormal flow patterns created as the blood flows from the graft into the artery, impinging on the bed of the junction.[6] Such flow behaviour is unphysiological, as end-to-side junctions do not occur naturally in adults. Thus, hemodynamic flow patterns in distal end-to-side anastomoses are widely implicated in the initiation of the disease formation processes.[7–10]

Intimal hyperplasia is known to be more evident with prosthetic grafts where it is concentrated at areas of flow disturbance around the distal anastomosis. Several factors have been implicated in the development of intimal hyperplasia including differences in the mechanical properties between prosthetic graft and native vessel[11] and low flow states due to poor run-off.[12] It is known that flow patterns created by end-to-side distal anastomoses exert abnormal wall shear stress (WSS) distributions on the endothelial cells on the bed of the junction.[13,14] The role of WSS in intimal thickening has been the subject of much debate with high WSS,[15] low WSS,[16] WSS gradient (WSSG)[17] and oscillating WSS[18] theories all being proposed as aetiological factors for anastomotic intimal thickening. These theories have been supported by experimental findings and it is possible that each theory has a role to play in the restenosis process.

Several vascular surgeons have achieved improved patency rates for polytetrafluoroethylene (PTFE)

*Corresponding author. T. McGloughlin, Mechanical and Aeronautical Engineering Department, University of Limerick, Limerick, Ireland. E-mail: tim.mcgloughlin@ul.ie

1078–5884/060649 + 08 $35.00/0

bypasses by using an interposition vein cuff[19] or patch.[20] One theory of how vein cuffs or patches may improve patency rates is by decelerating the flow, thereby reducing peak WSS and relaxing WSSGs,[19,20] thereby reducing intimal hyperplasia growth factors. As a result it is commonly perceived that an optimum graft–artery junction geometry may exist. This study used computational fluid dynamics (CFD) to analyse the flow patterns associated with specific graft–artery junction geometries in three-dimensional models. This experimental system was used to determine the influence of the angle between the impinging flow and the junction bed on the WSS distributions in the junction area.

Materials and Methods

The 'artery' in all idealised models is 100 mm long with the heel of the junction located 33 mm from the end of the proximal outflow segment (POS). The 'graft' is 50 mm in length. The first idealised model, the 45° geometry (Fig. 1(A)) was developed using two intersecting 6 mm conduits with an internal angle of 45°.[21,22] The second idealised geometry, the cuffed geometry (Fig. 1(C)) includes a cuff between the graft and the host artery. The cuff length was constrained to the length between the heel and toe of the 45° model, approximately 8.5 mm. The cuff height was set at 5 mm. The patched geometry model (Fig. 1(D)) is also an extension of the 45° model with a patch included at the graft–artery junction to modify the junctional geometry. The distance between the heel and toe of the patched model was set at 20 mm with an internal patch angle of 32°.

The use of realistic geometries may yield results that more accurately represent the WSS distributions present in distal anastomoses. Methods for the development of these realistic geometries include the use of MRI in vivo[23] and the use of CT-scans ex vivo.[24] In this study, the principle geometrical characteristics of a realistic graft–artery junction were obtained from a 3-month post-operative angiogram (see Fig. 2(A)). This femoro-popliteal anastomosis was chosen as it displayed a particularly well-defined 'bulb' at the junction. The geometry was extracted under the following assumptions:

- All cross-sections are diameters.
- The angiogram was taken in the plane of the graft–artery junction.
- There was no out-of-plane curvature.
- The 'bump' located distal to the toe on the junction side of the distal outflow segment (DOS) is ignored.

The resulting geometry, the realistic model (Fig. 2(B)) was scaled to give an average diameter of 6 mm, to maintain comparable flow rates to the idealised models presented above. The artery has a length of 30 mm with the heel of the junction located 12 mm from the end of the POS. The graft length is 20 mm. The realistic geometry illustrates the geometric features, which are not seen in idealised models. The bulb-like effect at the graft–artery junction is quite striking. The diameter of the POS and the DOS vary with axial location. The axial direction of the DOS also varies. Importantly, analysis of the flow patterns through the realistic geometry allows assessment of the influence of idealising the geometry on the junction flow patterns.

Computational fluid dynamics

Flow patterns within end-to-side anastomosis configurations were simulated using a commercially available CFD package (FLUENT, Europe). Three-dimensional models were developed using Pro-Engineer (Parametric Technology Company) and subsequently exported into Geomesh, a grid generation package (FLUENT, Europe), for grid generation. Numerical simulations used a non-Newtonian fluid model[25] and time-dependent in-flow boundary conditions. Rigid walls and zero flow in the POS were assumed.[21] It was also assumed that there was no out-of-plane curvature in any of the models. The resting pulse used in this study is characteristic of a femoral artery pulse. This pulse had a frequency of 1 Hz, a Womersley parameter of 4.2, which represents the pulsatile conditions and a mean Reynold's number equal to 180. For the time-dependent flow models time step independence was established at 0.01 s. The results are presented for the mean velocity in the deceleration phase of the femoral pulse used.[26] The numerical model used in this study was previously validated using laser Doppler anemometry studies.[26]

Wall shear stress normalisation

The process of normalising the WSS allows results from different models to be compared directly with each other allowing easy identification of any differences. Eq. (1) defines normalised WSS.

$$\tau_n = \tau_z/\tau_{z_a} \tag{1}$$

where τ_n, normalised WSS; τ_z, WSS; τ_{z_a}, average WSS far down stream in the model; z, distance along the bed of the junction in the proximal to distal direction.

In addition, it is proposed that the variation of the

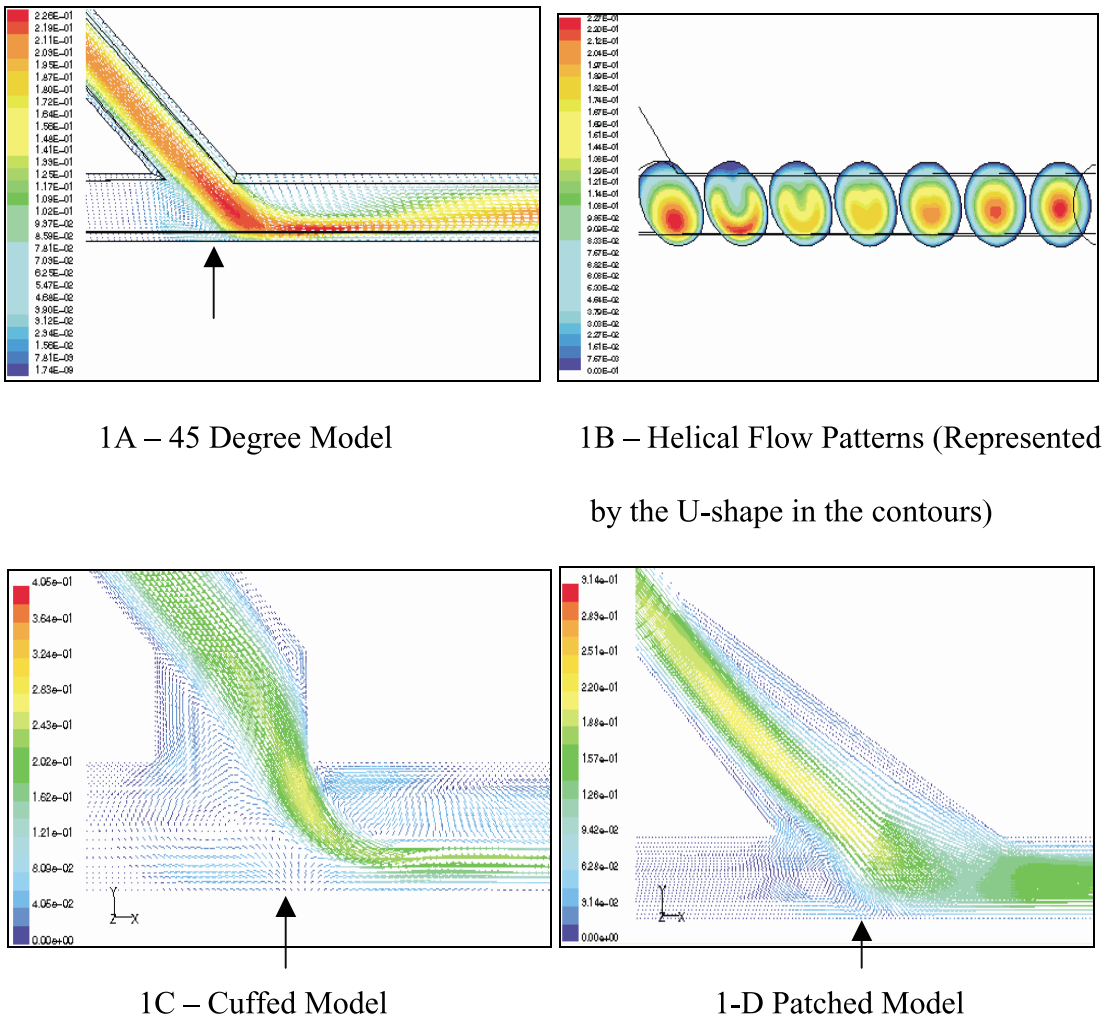

Fig. 1. Illustration of the flow patterns through the centrelines of conventional (1A), cuffed (1C) and patched (1D) idealised end-to-side graft–artery junctions (arrows indicate the location of the bed stagnation point (BSP)).

local gradient in shear stress on the junction bed could be used as an improved indicator of abnormal forces acting on the bed at an endothelial cell level. The slope of the WSS distribution is taken on a computation cell-to-cell level and divided by the distance between the two cell centre points. The slope is then normalised by dividing the value by the average WSS on the bed centreline of that model and multiplied by the average radius of the model.

$$\tau_g = \left[\frac{\mathrm{d}\tau_z}{\mathrm{d}z} / \frac{\tau_{z_a}}{r_a} \right] \quad (2)$$

where τ_g, normalised spatial WSSG; τ_z, WSS; τ_{z_a}, average WSS on the bed centreline in the host artery for all models; r_a, average radius of the model.

Results

Qualitative results

The qualitative results for each of the geometries are similar. Recirculation regions are found opposite the heel and distal to the toe of the junction in all models (Figs. 1(A), (C), (D) and 2(C)). Flow impinges on the junction bed creating a bed stagnation point (BSP). As the flow moves distally through the DOS the momentum of the fluid causes it to follow the vessel wall curvature creating helical flow patterns in the DOS (Fig. 1(B)).

The flow enters the host artery in the 45° model at an angle of 45° (Fig. 1(A)). The flow impinges on the bed of the host artery and recovers in the DOS. By allowing the flow to enter the host artery through a divergent section and effectively a lower angle in the

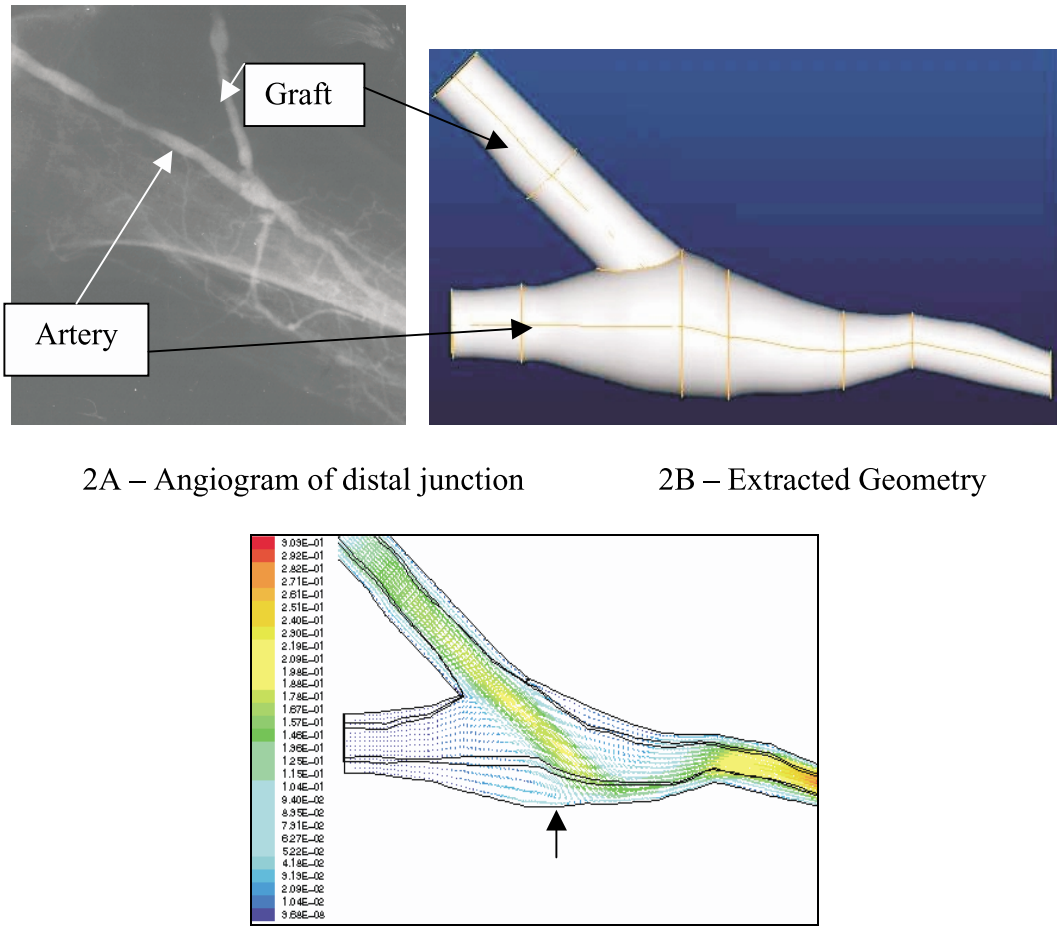

Fig. 2. Illustration of the angiogram and resulting geometry for Model 3 (arrow indicates the location of the bed stagnation point (BSP)).

patched model, (Fig. 1(D)) the force of the impinging flow on the artery bed is reduced. Inclusion of a patch in the junction also results in weaker heel recirculation, (Fig. 1D) albeit through a larger region than that in the 45° model. Also, there is reduced strength of the helical flow patterns. Allowing the flow to enter the host artery via a cuff effectively increases the flow impingement angle on the artery bed. The use of a cuff creates a large recirculation located within the cuff itself which serves to reduce the force of the impinging flow on the bed of the junction (Fig. 1(C)).

In the realistic model, Fig. 2(C) it is noted that the highest velocities are located at the exit of the DOS due to the small diameter at the DOS outlet segment. Large recirculation regions can be seen opposite the heel and distal to the toe of the junction. The effect of the changing direction of the DOS on the flow is seen with another point of flow impingement being located further downstream in the DOS. It can be seen that the effect of the bulb in the junction geometry is to keep the flow from impinging on the artery bed until it has moved significantly into the DOS (Fig. 2(C)). Weak helical flow patterns are formed in the DOS since the momentum of the fluid is reduced as it moves from a small diameter graft into the large junction area.

Quantitative results

Analysis of the quantitative results from the three geometries reveals significantly different results. Fig. 3 shows the WSS distributions on the centreline of the arterial bed for each of the models. Comparing the WSS distributions for the 45° and the patched geometries, the effect of increasing the junctional area and effectively reducing the graft–artery junction angle can be seen. The inclusion of a patch moves the BSP distally, increasing the area on the bed of the junction, which experiences a BSP. The BSP is the point

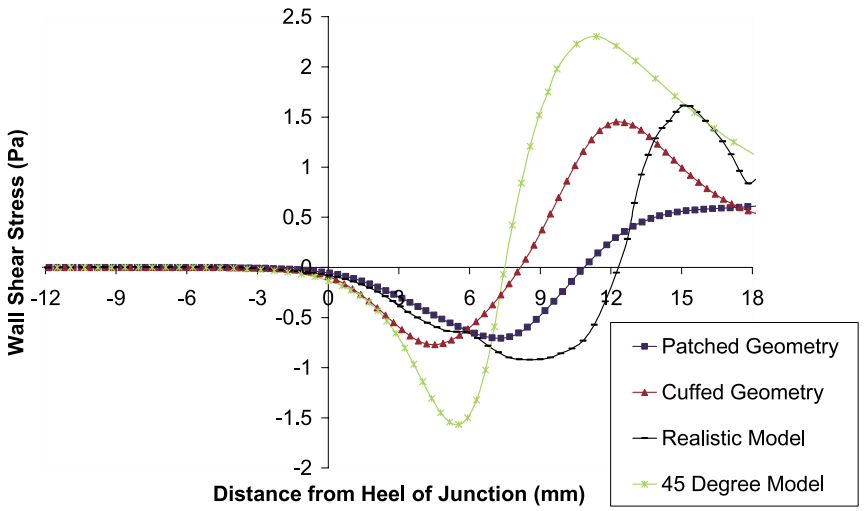

Fig. 3. The WSS distributions on the centreline of the arterial bed for each of the models.

on the artery bed where the flow splits proximally and distally. For the two models in question the BSP moves an extra axial distance of 3.2 mm, an increase in distal location of 43%. Also, the inclusion of a patch reduced the velocity of the flow (peak negative WSS) in the recirculation region opposite the heel of the junction by 54.8%.

The increased junctional area leads to an increase in axial size of the recirculation region of 43%. The inclusion of a patch significantly reduces the peak WSS, by 72%. The location of the peak WSS is found at an axial distance of 9.4 mm or 45.2% further downstream for the patched geometry than the peak WSS for the 45° geometry. The smaller junction area and effectively larger graft–artery angle of the 45° model promotes earlier recovery of the flow in the DOS than for the patched geometry. However, the associated helical flow patterns in the DOS are stronger. Conversely, the weaker helical flow patterns associated with the patch geometry persist further downstream from the junction.

Comparing the WSS distributions for the 45° and the cuffed geometries the effect of increasing the junctional area but effectively increasing the graft–artery junction angle can be seen. The inclusion of a cuff also moves the BSP distally, again increasing the area on the bed of the junction, which experiences a BSP. The cuffed geometry moves the BSP an extra axial distance of 0.7 mm distally. Also, the inclusion of a cuff reduced the velocity of the flow in the recirculation region opposite the heel of the junction by 50.8%. The increase in graft–artery angle leads to an increase in axial size of the recirculation region of 9.5%. The location of the peak WSS is found at an axial distance of 0.94 mm or 8.1% further downstream for the cuffed geometry than the peak WSS for the 45° geometry. However, the larger junction area and effectively larger graft–artery angle promotes earlier recovery of the flow in the DOS than for the 45° model. Also, the helical flow patterns in the DOS associated with the cuff geometry are stronger.

The WSS distributions for the realistic geometry can also be seen in Fig. 3. The profile shows a constantly varying WSS distribution. Comparing the WSS distributions for the 45° and the realistic geometries, again the effect of increasing the junctional area and effectively reducing the graft–artery junction angle can be seen. In the junction area, up to 18 mm from the heel, the qualitative results for the realistic geometry follow those of the cuffed geometry. The bulb effect in the artery of the realistic geometry serves to slow the flow and moves the BSP away from the junction. The varying diameter and axial direction of the DOS result in the fluctuating WSS distribution seen in Fig. 3.

These WSS results are analysed and presented as both normalised WSS distributions and normalised WSSG distributions.

Normalised WSS distributions for each model

Fig. 4 presents the normalised WSS distributions for each of the models. This is the most commonly used method of results presentation for WSS distributions.[5,26] However, normalising the WSS distributions does not change the profiles of the distributions. Overall the results are essentially the same as for the WSS distributions presented above in Fig. 3.

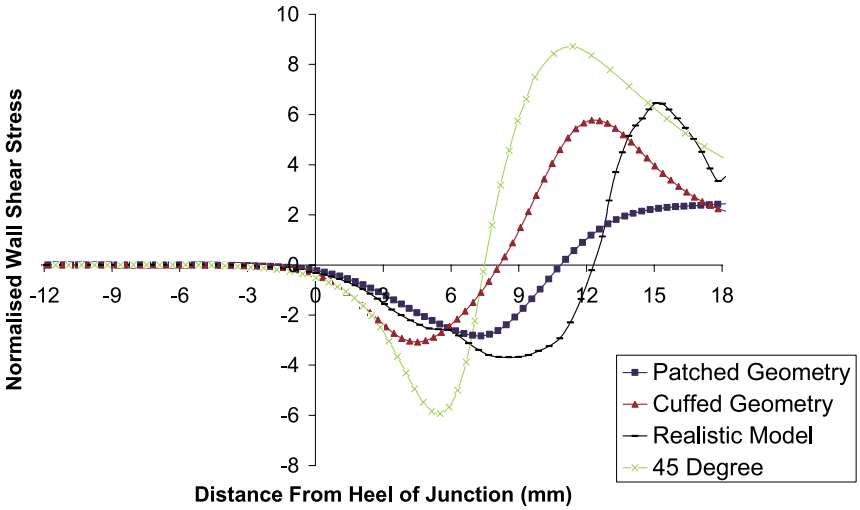

Fig. 4. The normalised WSS distributions on the centreline of the arterial bed for each of the models.

Normalised WSSG distributions for each model

Fig. 5 shows the normalised local spatial axial WSSG distributions for the bed of each model. Normalised WSSG distributions may prove to be a better predictor of the initiation of the disease formation processes on the bed of the junction.[17,21] Comparing the distributions for the 45°, patched and cuffed geometries, it can be seen that the effect of including a patch or cuff has a significant effect on the normalised WSSG distribution. The peak values shown for the 45° geometry are approximately three times those which are shown for the patch and cuff geometries. This demonstrates the abrupt change in local WSS in the 45° model as opposed to the gradual change in local WSS seen in the patched and cuffed geometries. The large variation in local WSS distributions becomes even more evident when looking at the realistic geometry. The normalised WSSG distribution for the realistic model demonstrates large fluctuations over the junction bed.

Discussion

Several assumptions were made when developing the numerical model for this study. Rigid walls and zero flow in the POS were assumed for simplicity. These assumptions have been shown to affect the quantitative nature on the results. However, the influence of compliance and proximal outflow on the flow field has been shown to be qualitatively

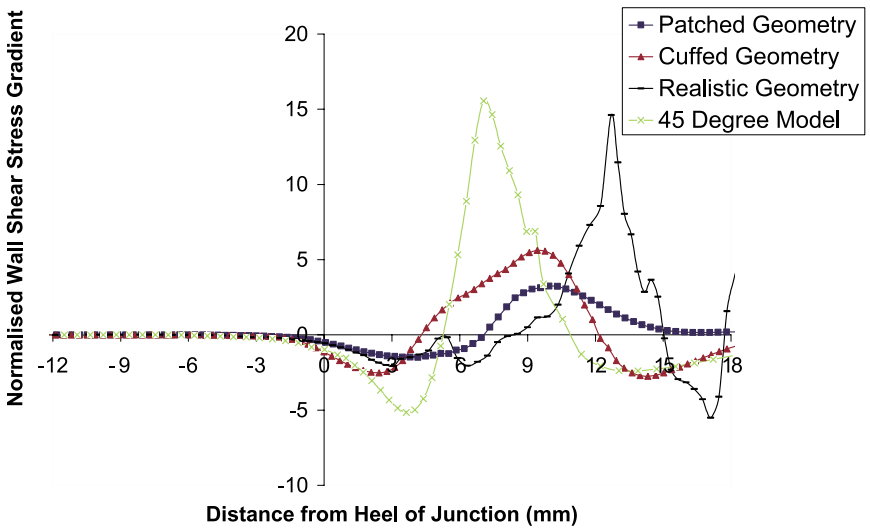

Fig. 5. The normalised WSSG distributions on the centreline of the arterial bed for each of the models.

small.[27] Also, out-of plane curvature has been shown to affect the quantitative nature of WSS distributions in graft–artery junction by up to 10%. Again, the qualitative nature of the results is similar to in-plane results.[28]

The improved patency of prosthetic PTFE infrainguinal bypasses by using an interposition vein cuff has led to a renewed interest in establishing factors that influence the development of intimal hyperplasia at the distal anastomosis.[29] Our results using CFD demonstrate the effects of distal anastomotic geometry on blood flow dynamic parameters including the location of the BSP, recirculation regions, helical flow patterns in the DOS and velocity profiles.

The realistic geometry model, Fig. 2, was generated to investigate the principal effects of two-dimensional wall curvature on the junction hemodynamics. It is suggested that arterial wall remodelling could be responsible for the unusual bulb at the junction. If so, it is possible that the optimisation of a graft–artery junction is not only a function of the geometry and blood characteristics, but also a function of how the artery will remodel itself in response to the altered flow patterns. Flow patterns inside idealised and realistic geometries were found to be similar.

Flow impinges on the bed of the host artery and recovers in the DOS. Although quantitative WSS distributions for a specific realistic geometry cannot be accurately predicted using idealised geometries, the qualitative attributes of the flow patterns associated with different geometric features can be. In a healthy idealised artery, the local spatial gradient of WSS is zero. Therefore, the deviation from zero of the normalised WSSG distribution, as seen in Fig. 5, represents the area in the junction bed where the endothelial cells (EC) experience abnormal WSSG, which could be the initiating factor for the disease formation processes. It is characteristic of distal bypass geometries to have non-zero normalised WSSG distributions. End-to-side anastomoses will always contain flow patterns, which have flow characteristics that include, a BSP, flow impingement, heel and toe recirculation, skewed velocity profiles and helical flow patterns in the DOS. Also, increasing the graft–artery junction area increases the area on the bed of the junction on which a BSP acts.

Comparing the normalised WSSG distributions for the realistic geometry in Fig. 5 to those for the idealised models, a large variation in local WSSG becomes evident. In the DOS the profile for the realistic geometry varies constantly as does the DOS direction and diameter. It can also be seen that the strong slope of the profiles at several of these axial locations indicate that large abrupt changes in local WSS take place at several points on the artery bed. These results may indicate that an ideal graft–artery junction geometry would reduce the number of locations on the artery bed which could experience large abrupt changes in local WSS. Fig. 3 shows that increasing the graft–artery junction area has the effect of reducing the peak WSS magnitudes. Fig. 5 shows that the increased area also reduces the WSSG. In both figures, it is evident that the realistic model has significantly different and essentially unpredictable WSS magnitudes and gradients.

The normalised WSSG distributions for the patch geometry return to a value less than 0.5 at an axial location 14.4 mm from the heel of the junction. The corresponding results for the cuffed and 45° geometries are 18.9 and 23.1 mm, respectively. Over the area of interest the realistic geometry does not resolve to within this value. The peak normalised WSSG values for the idealised geometries are 15.55, 2.52 and 1.49 for the 45°, cuffed and patched geometries, respectively. This implies that using patched and cuffed geometries impose significantly less gradients of stress on the EC on the junction bed.

The results of this study provide evidence that altering the flow patterns within end-to-side vascular anastomoses could yield improved patencies by two potential mechanisms. In terms of this study these mechanisms would be reducing the peak values in the normalised WSSG distribution or reducing the area over which the normalised WSSG distribution has a non-zero value. The patch technique appears to reduce the peak values of the normalised WSSG distributions while the vein cuff minimises the axial distance for which the normalised WSSG distribution has a zero value. Both cuff and patch techniques have only moderate long-term patency rates,[20,30] as do all infrainguinal bypass grafts. Therefore, we speculate that an optimum end-to-side graft–artery junction geometry, which would significantly increase the patency rates of peripheral bypass surgery, has yet to be determined and possibly may not exist.

Conclusions

Both quantitative and qualitative WSS distributions on the bed of graft–artery junctions are influenced by graft–artery angle and by idealising the geometry. Normalised WSSG distributions emphasise important bed locations where significant gradients of shear occur. These areas may be overlooked using normalised WSS distributions. Idealised geometries can be used to determine the approach to design an optimum graft–artery junction. CFD analysis may not take into

account several additional mechanical factors such as the influence of graft–artery diameter ratios or the presence of vortices within the vein cuff.[31] Therefore studies using in vitro models will be necessary for further validation of these results. In addition, studies designed to assess the response of endothelial cells to specific WSSG are required to provide insight into proven and experimental approaches that would improve the design of graft–artery junctions.

Acknowledgements

The authors would like to acknowledge Enterprise Ireland and Materials Ireland for their support.

References

1 Whittemore AD, Clowes AW, Couch NP, Mannick JA. Secondary femoropopliteal reconstruction. *Ann Surg* 1981; **193**: 35–42.
2 Neville RF, Sidawy AN. Myointimal hyperplasia: basic science and clinical considerations. *Semin Vasc Surg* 1998; **11**: 142–148.
3 Steinman DA, Moore JA, Martin AJ. The effect of flow waveform on anastomotic wall shear stress patterns. *Adv Bioengng, BED* 1995; **31**: 173.
4 Loth F. Wall shear stress measurements inside a vascular graft model under pulsatile flow conditions. *Bioengng Conf, BED* 1995; **29**: 9–10.
5 Ethier CR, Moore JA, Steinman DA, Martin AJ, Rutt BK. Flow simulations in a physiological arterial bifurcation. *ASME Bioengng Conf, BED* 1995; **29**: 471–472.
6 Staalsen NH, Ulrich M, Winther J *et al.* The anastomosis angle does change the flow fields at vascular end-to-side anastomoses in vivo. *J Vasc Surg* 1995; **21**: 460–471.
7 Noori N, Scherer R, Perktold K *et al.* Blood flow in distal end-to-side anastomoses with PTFE and a venous patch: results of an in vitro flow visualisation study. *Eur J Vasc EndoVasc Surg* 1999; **18**: 191–200.
8 Kleinstreuer C, Lei M, Archie JP. Hemodynamics of a femoral graft artery connector mitigating restenosis. *Adv Bioengng, BED* 1995; **31**: 171–172.
9 Friedman MH. Arterial geometry affects hemodynamcis. *Atherosclerosis* 1983; **46**: 225–231.
10 Giddens DP, Zarins CK, Glagov S. The role of fluid mechanics in localisation and detection of atherosclerosis. *J Biomech Engng* 1993; **115**: 588–594.
11 Miyawaki F, How TV, Annis D. Effect of compliance mismatch on flow disturbances in a model of an arterial graft replacement. *Med Biol Engng Comput* 1990; **28**: 457–464.
12 Kohler TR, Kirkman TR, Kraiss LW *et al.* Increased blood flow inhibits neointimal hyperplasia in endothelialised vascular grafts. *Circ Res* 1991; **69**: 1557–1565.
13 Xiao Y, Truskey GA. Effect of flow recirculation upon endothelial cell height and shape. *Bioengng Conf, BED* 1997; **35**: 537–538.
14 White SS. Hemodynamics patterns in two models of end-to-side vascular graft anastomoses: effects of pulsatility, flow division, Re. No. and hood length. *J Biomech Engng* 1993; **115**: 104–111.
15 Fry DL. Responses of the arterial wall to certain physical factors. In: Porter R, Knight J, eds. *Atherosclerosis: Initiating Factors*. Amsterdam: Associated Scientific Publisher, 1973: 93–125.
16 Caro CG, Fitz-Gerald JM, Schroter RC. Atheroma and arterial wall observations, correlation and proposal of a shear dependent mass transfer mechanism for atherogenesis. *Proc R Soc London, Ser B* 1971; **177**: 109–159.
17 Kleinstreuer C, Lei M, Archie JP. Flow input waveform effects on the temporal and spatial wall shear stress gradients in a femoral graft–artery connector. *J Biomech Engng* 1996; **118**: 506–510.
18 Taylor CA, Hughes TJ, Zarins CK. Effect of exercise on hemodynamic conditions in the abdominal aorta. *J Vasc Surg* 1996; **29**: 1077–1089.
19 Raptis S, Miller JH. Influence of vein cuff on polytetrafluoroethylene grafts for primary femoropoliteal bypass. *Br J Surg* 1995; **82**: 487–491.
20 Taylor RS, Loh A, McFarland RJ *et al.* Improved technique for polytetrafluoroethylene bypass grafting: long term results using anastomotic vein patches. *Br J Surg* 1992; **79**: 348–354.
21 Ethier CR, Steinman DA, Zhang X, Karpik SR, Ohja M. Flow waveform effects on end-to-side anastomotic flow patterns. *J Biomech* 1998; **31**: 609–617.
22 Lei M, Archie JP, Kleinstreuer C. Hemodynamic simulations and computer-aided designs of graft–artery junctions. *J Biomech Engng* 1997; **119**: 343–348.
23 Milner JS, Moore JA, Rutt BK, Steinman DA. Hemodynamics of human carotid artery bifurcations: computational studies with models reconstructed from magnetic resonance imaging of normal subjects. *J Vasc Surg* 1998; **27**: 143–156.
24 Perktold K, Hofer M, Rappitsch G, Loew M, Kuban BD, Friedman MH. Validated computation of physiologic flow in a realistic coronary artery branch. *J Biomech* 1998; **31**: 217–228.
25 Cho YI, Kensey KR. Effects of the non-Newtonian viscosity of blood on flow in a diseased arterial vessel. Part 1: steady flows. *Biorheology* 1991; **28**: 241–262.
26 Walsh M, McGloughlin T, Liepsch DW, O'Brien T, Morris L, Ansari AR. On using experimentally estimated wall shear stresses to validate numerically predicted results. *Proc ImechE* 2003; **217**(Part H): 77–90.
27 Leuprecht A, Perktold K, Prosi M, Berk T, Trubel W, Schima H. Numerical study of hemodynamics and wall mechanics in distal end-to-side anastomoses of by-pass grafts. *J Biomech* 2002; **35**: 225–236.
28 Papaharilaou Y, Doorly DJ, Sherwin SJ. The influence of out-of-plane geometry on pulsatile flow within a distal end-to-side anastomosis. *J Biomech* 2002; **35**: 1225–1239.
29 Stonebridge PA, Prescott RJ, Ruckley CV. Randomized trial comparing infrainguinal polytetrafluoroethylene bypass grafting with and without vein interposition cuff at the distal anastomosis. *J Vasc Surg* 1997; **26**(4): 543–550.
30 Kansal N, Pappas PJ, Gwertzman GA *et al.* Patency and limb salvage for polytetrafluoroethylene bypasses with vein interposition cuffs. *Ann Vasc Surg* 1999; **13**: 386–392.
31 Harris P, How T. Haemodynamics of cuffed arterial anastomoses. *Crit Ischaemia* 1999; **9**: 20–26.

Accepted 6 August 2003